Spins, magnetic moments, and isotope shifts of $^{21-31}$Na by high resolution laser spectroscopy of the atomic D_1 line

G. Huber,† F. Touchard, S. Büttgenbach,†† C. Thibault, and R. Klapisch
Laboratoire René Bernas du Centre de Spectrométrie Nucléaire et de Spectrométrie de Masse, 91406 Orsay, France

H. T. Duong, S. Liberman, J. Pinard, J. L. Vialle, P. Juncar, and P. Jacquinot
Laboratoire Aimé Cotton, Centre National de la Recherche Scientifique II, 91405 Orsay, France
(Received 22 June 1978)

A polyisotopic sodium beam produced by reactions of 20 GeV protons in an uranium target, was illuminated with a tunable cw dye laser. The atomic beam is analyzed by a six-pole magnet, ionized, and detected after selection of one isotope by use of a mass spectrometer. From the optical D_1 resonance lines the hyperfine structure, magnetic moments, and isotope shifts of $^{21-31}$Na have been determined. The nuclear spins of $^{26-30}$Na have been measured by magnetic resonance. The results are discussed in terms of nuclear deformation. The analysis of isotope shifts shows the presence of an appreciable volume shift contribution.

[NUCLEAR STRUCTURE $^{26-30}$Na; measured J. $^{21-31}$Na; measured isotope shifts; deduced μ. Atomic beam laser spectroscopy and magnetic resonance.]

I. INTRODUCTION

The study of nuclear masses of exotic, neutron-rich sodium isotopes by on-line mass spectrometry had shown irregularities in the two neutron binding energy at $N=20$, which can be interpreted in terms of nuclear deformation.[1,2] Within the framework of a more detailed investigation of these isotopes, new mass measurements,[3] β-, γ-spectroscopy measurements,[4] and the present optical measurements have been performed at the proton synchrotron (P.S.) at CERN. Spins, magnetic moments, and isotope shifts of a long sequence of isotopes are of obvious interest to nuclear structure. At present full s-d shell calculations using different effective forces are available[5] and also Hartree-Fock calculations using a Skyrme effective force have been published on these nuclei.[2] Both calculate binding energies and spins or deformation parameters, respectively. But, to our knowledge, no magnetic moment calculations on neutron-rich sodium isotopes have been reported.

In this detailed report on the optical investigations we present in Sec. II the principle of the experiment, in Sec. III the experimental set up, in Sec. IV the experimental procedure, and in Sec. V the results and their interpretation using the Nilsson model and the classical theory of isotope shift.

II. PRINCIPLE OF THE EXPERIMENT

The experimental set up uses a method of non-optical detection of optical resonances by means of magnetic deflection. This method has been developed and applied to $^{21-25}$Na at Orsay.[6-8] A target, placed inside a high temperature oven, is bombarded with a proton beam. The thermalized reaction products are emitted from the oven and form an atomic beam [Fig. 1(a)]. In the 1 region the sodium atoms may be excited by a light beam of a cw tunable single mode dye laser, in presence of a small magnetic field. At optical resonance with one of the well resolved hyperfine components of the D_1 line, hyperfine optical pumping occurs and changes the population distribution between the magnetic substates m_F. The atomic states pass adiabatically from the weak field region (interaction region) to the strong field region (inside the six-pole magnet), where I and J are decoupled. The atoms have then $m_J=+\frac{1}{2}$ or $m_J=-\frac{1}{2}$. The six-pole magnet (2 region) focuses the atoms with $m_J=+\frac{1}{2}$ and defocuses the atoms with $m_J=-\frac{1}{2}$. A signal proportional to the number of focused atoms of the studied sodium isotope is obtained by counting them with an electron multiplier after they have been ionized and passed through a mass spectrometer. The signals observed when scanning the laser frequency are shown in Fig. 1(b).

In this experiment, the light propagates along the direction of a small magnetic field H_0 perpendicular to the atomic beam. The field is small enough so that the total width of the Zeeman splitting of the line is smaller than 10 MHz, the natural line width. Π excitation is excluded. The calculation of the optical pumping for σ excitation is complicated because of coherence effects. The theory for the simple case of pure polarization (σ^- or σ^+) is given in Appendix A. A program has been written to compute the evolution of the populations using the optical pumping matrix from Appendix A. For $I=\frac{3}{2}$(^{23}Na) the result as a function of $W\cdot t$, W being the light power density and

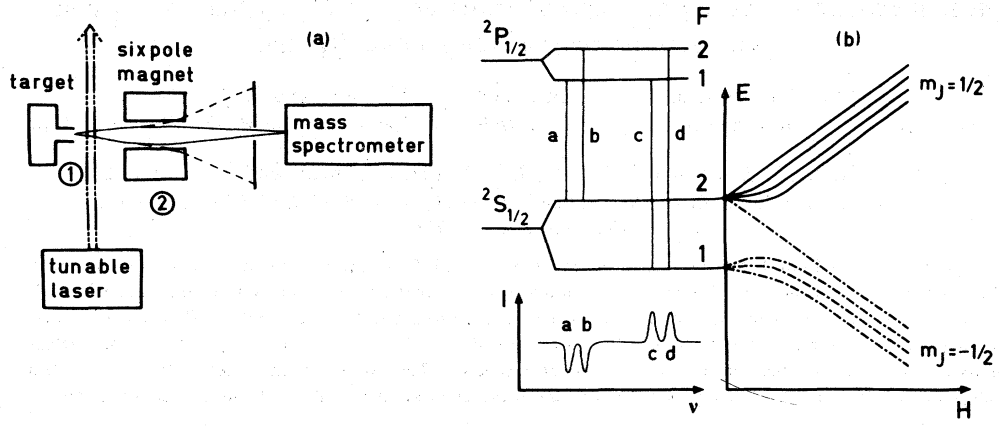

FIG. 1. (a) Scheme of the experiment. (b) Signals with the D_1 line for $I=\frac{3}{2}$.

t the interaction time, is shown in Fig. 2. From this figure if can be seen that there is a value of W for which the resonance signal approaches its asymptotic value. An increase in W would only broaden the resonance signal. The optimal value of W depends on the light polarization and on the hyperfine component, as well as on the nuclear spin. Therefore, ideally, W should be adjusted for each case. Since in practice a light power density range around the optimal value can be tolerated, we used , for reasons of time sparing, the same value of a few mW/cm^2 which is in the tolerable range of all cases (see Fig. 2).

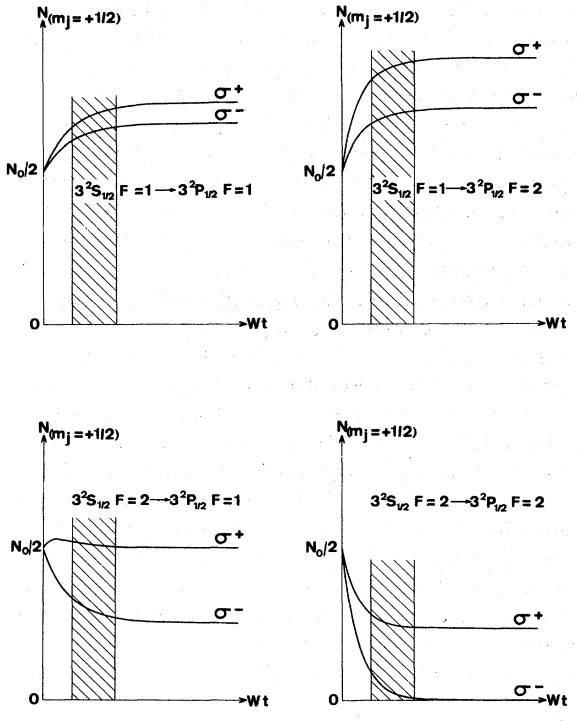

FIG. 2. Optical pumping with polarized light.

In order to determine the nuclear spin I we used the well known magnetic resonance method. The laser light is polarized σ^- and frequency locked to the hyperfine transition $^2S_{1/2}, F=I+\frac{1}{2} \rightarrow {}^2P_{3/2}$, $F'=I+\frac{3}{2}$. Zeeman pumping occurs and the populations of the ground state sublevels are changed. The atoms involved in this transition are pumped in the Zeeman sublevel $m_F=-(I+\frac{1}{2})$ of the $F=I+\frac{1}{2}$ hyperfine ground state. Consequently all atoms are defocused by the six-pole magnet. A rf field perpendicular to the static field H_0 is applied to the optically pumped atoms. If the rf frequency is equal to the frequency of the transition between two adjacent Zeeman sublevels, the rf field tends to equalize the populations of all Zeeman sublevels since H_0 is weak enough for the Zeeman effect to be linear. In our case, the population of the $m_F=-(I+\frac{1}{2})$ sublevel is redistributed into Zeeman sublevels of the $F=I+\frac{1}{2}$ hyperfine ground state. The transferred atoms are focused by the six-pole magnet and the detected signal increases.

The transition frequency between two adjacent Zeeman sublevels in weak magnetic field H_0 is given by

$$\nu = g_F \mu_B H_0/h$$

where

$$g_F = \frac{F(F+1)+J(J+1)-I(I+1)}{2F(F+1)} g_J .$$

A term in g_I has been neglected in this expression, since $g_I \ll g_J$. In the case $J=\frac{1}{2}, g_J=2$ the transition frequency is

$$\nu = \frac{2\mu_B H_0}{(2I+1)h} .$$

For a given rf frequency ν_{rf} and for each possible value of I there is a value of H_0 for which the

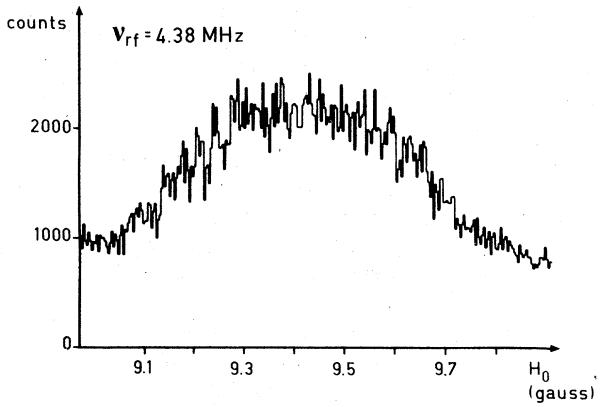

FIG. 3. Magnetic resonance signal for spin measurement of ^{25}Na.

transmitted beam intensity must increase

$$H_0 = \frac{\nu_{rf} h(2I+1)}{2\mu_B} .$$

The nuclear spin I is measured by checking which of these discrete values of H_0 produces an increase of the signal. The signal obtained on ^{25}Na by sweeping the magnetic field H_0 is shown in Fig. 3. The same Zeeman pumping effect occurs in the D_1 line, although the signal at rf resonance is smaller. Since the D_1 line was used for hyperfine structure and isotope shift measurements, it was more convenient to use the D_1 line also for the spin measurements.

III. APPARATUS

A. The uranium target and the atomic beam set up

It is now well known that neutron-rich light nuclei can be produced by bombarding an uranium target with high energy protons (see e.g. Refs. 9, 10). The target structure has already been described,[10] and the cross sections for the production of sodium isotopes have been measured.[10,11] A thin layer of ^{238}U is deposited on graphite foils. The recoil fragments produced by the nuclear reactions are implanted into the graphite. There, a chemical separation is achieved by the selective diffusion of the alkali atoms through the graphite as they come out of the target very quickly and form a thermal atomic beam.

Uranium dioxide powder from a suspension in amyl-acetate is sedimented (≈15 mg/cm^2) on graphite foils 50 μm thick and 45 × 5 mm^2 surface. 20 foils, separated by 100 μm graphite spacers, were glued into a stack with two 500 μm cover foils of graphite (Fig. 4). After sintering by heating up to 2000°C in vacuum, the stack was inserted in the tantalum oven. It was placed with the 4 × 5 mm^2 face toward the proton beam. According to recoil energy measurements,[9] about 60% of the produced sodium should be transferred to the graphite foils. The oven consists of a 300 μm thick tantalum foil rolled to form an 8 mm diameter and 50 mm long cylinder. Current connections are spotwelded at the top leads. In the middle of this tube a 3 mm diameter tube was spotwelded at right angle as an atomic beam exhaust. In order to increase the directivity of the emission of atoms, 3 collimating channels, 1 mm diameter and 20 mm long were inserted in the beam exhaust tubing. The exhaust tubing is provided with a current connection so that separate heating of the main part of the oven and the outlet tubing is possible. After heating to 2000°C, no change in the initial alignment of the oven, with respect to both the proton beam and the atomic beam axis was observed, due to the symmetrical and flexible construction of the current connections which support the oven. The purpose of the high temperature is to allow a fast diffusion of the sodium atoms through the graphite and the exhaust tubing. This allows us to study the short-lived sodium isotopes with $A \geq 28$ (see Sec. III E).

The region where the atoms interact with the laser light was magnetically shielded. The small static magnetic field H_0 was produced by a solenoid placed inside the shielding. The rf field was produced by a 10 turns solenoid centered on the atomic beam axis. Care has been taken to maintain a small field of the same direction than H_0 inside the magnetic shielding in order to avoid nonadiabatic transitions.

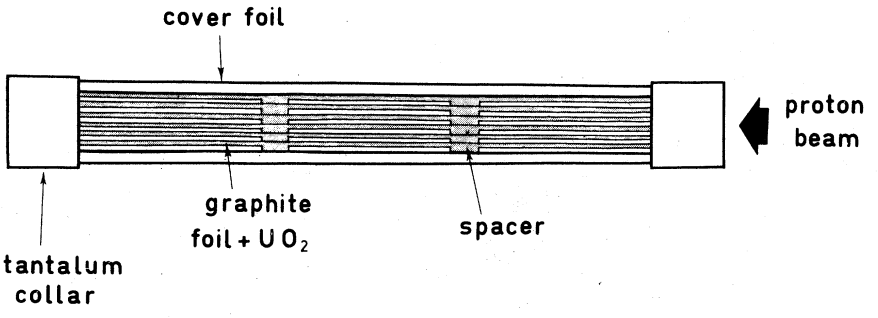

FIG. 4. Schematic view of the uranium graphite target.

B. The dye laser

Since contributions of the volume effect in the isotope shift were expected to be of the order of a few MHz, the frequency of the D_1 line had to be measured with an accuracy of about 10^{-8}. For this purpose we built a frequency controlled dye laser system. As in previous experiments[7,8] this system comprised a "sigmameter"[12] which permits us both to stabilize the laser frequency and to scan it step by step with increments as small as 1 MHz.

The general scheme of the set up is shown in Fig. 5. A commercial dye laser system (CR 599) operated on one single mode whose frequency is locked using a reference Fabry-Perot cavity. The frequency jitter is less than 1 MHz; it is continuously tunable over a range of 30 GHz. But the stability is only 10 MHz per hour, so that a more stable reference is needed. For this purpose a small part of the laser light is sent into the sigmameter, which consists of a Michelson type interferometer with a fixed path difference of $\delta = 200$ cm, which is servocontrolled by use of a wavelength standard laser line. The common phase of the two normalized interference signals $\sin\phi$ and $\cos\phi(\phi = 2\Pi\sigma\delta)$, provided by the sigmameter, can be vizualized on a X-Y scope (Fig. 5), and by electronic comparison with a reference phase an error signal for the CR 599 frequency control system is generated. Thus the laser frequency, i.e., its wave number σ is stabilized on the sigmameter: the reference phase can be scanned in discrete steps of $\Delta\phi = 2\Pi \times p/160$, where p is a chosen integer. The minimum increment $(p = 1)$ is then $\Delta\sigma = 1/160.200$ cm^{-1} or $\Delta\nu = 0.9375$ MHz. In order to obtain a good optical stability of the sigmameter a Koster prism has been used for the multiple functions of beam splitter, compensator plate, mirror, and dephasing element, as one face of the prism has a reflective metal coating (see Fig. 5). The second mirror of the interferometer is mounted 1 m apart from the Koster prism by means of invar spacers and a piezoceramic stack.

A He-Ne laser locked on an iodine saturated absorption line is used to servocontrol the path difference δ. The He-Ne laser light path inside the interferometer is parallel to the dye laser light. The interference fringes generate an error signal in a servoloop acting on the piezoceramic stack of the second mirror. The stability of the whole system has been studied using the D_1 line of stable sodium (^{23}Na) whose hyperfine structure is known very accurately. This experiment is done by detecting the fluorescence signal from a well collimated atomic beam which is illuminated with the laser light. The results have shown a stability over several hours as well as a reproducibility of better than 1 MHz. This fluorescence signal of natural sodium was used as a reference frequency for the isotope shift measurements of $^{21\text{-}31}$Na.

To avoid first order Doppler frequency shifts of the resonance due to deviation from perfect perpendicularity between the atomic beam and the laser beam axis, the light was reflected back on itself on the radioactive atomic beam as well as on

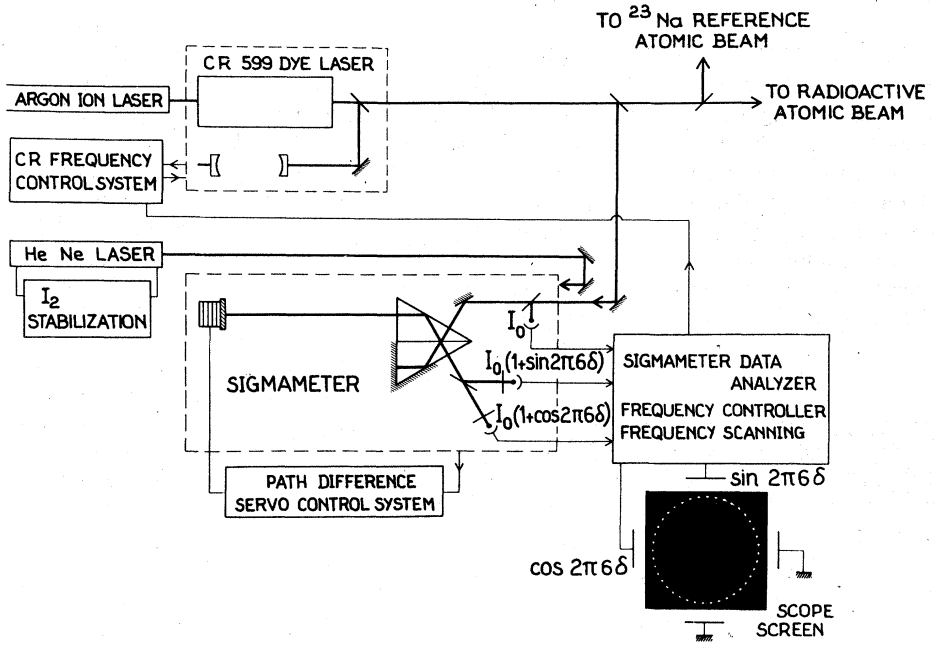

FIG. 5. General scheme of the laser set up.

the reference ^{23}Na beam. However, the retroreflection is not perfect in order to avoid light reflection into the dye laser. From the achieved angle between the two light beams we have found that a residual frequency shift of about ±1 MHz was to be expected. In fact, the systematic error introduced by this residual shift in the mean value of the isotope shift measurements is less than 1 MHz, due to different settings of retroreflection.

C. The six-pole magnet

We used two commercial six-pole magnets in series as magnetic state selector, each with 9300 Gauss at the pole tips, 8.6 cm length and 0.32 cm gap diameter. Calculating the transmission as described in Appendix B, a program has been written to determine the optimal value for L, assuming that the sodium atoms emerging from the oven are themalized at 2000 °K. We found with $L = 6$ cm the separation parameter s, defined in Appendix B, to be 80%, and the effective solid angle to be $4.5\ 10^{-4}$sr, about three times the solid angle defined by the magnet exit and the beam source. Taking into account the dimension of the oven aperture, the collimation of the beam is 40, leading to a width of the optical resonance of about 70 MHz. The observed width is somewhat larger (100 MHz) due to saturation of the optical pumping process.

D. The mass spectrometer

After the interaction with the laser beam and the state analysis through the six-pole magnet, the alkali isotopes are separated by a mass spectrometer. The required ionization—achieved by a rhenium surface ionizer—reinforces the chemical selection, since the alkali metals are well known for their low ionization potential when compared to neighboring elements. Since the ionization potential of sodium 5.14 eV is comparable to the work function of rhenium 5.1 eV only about 30% of the atoms can be ionized. To increase the ionization efficiency a small flow of oxygen was continuously directed on the ionizer. This led to the formation of rhenium oxide and thus brought the ionization efficiency close to unity.[13] This was achieved by a controlled air leak near the ion source. The mass spectrometer has an inhomogeneous field (angle $\Phi = 90°$, field index $n = 0.23$, radius $R = 35$ cm) providing a resolving power which may be adjusted to values ≤ 650. Its transmission has been measured using a chopped atomic beam of ^{23}Na. The ratio of the intensities before the ionizer (i.e., the source of the spectrometer) and at the detector placed at the end of the ion transport line is measured to be 50–75%, for a mass resolution $M/\Delta M$ of the order of 300.

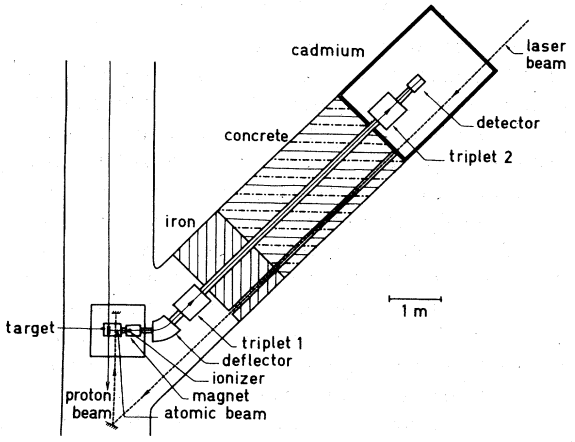

FIG. 6. Overall view of the experimental area.

The beam at the P.S. consists of very short (2.1 μs) pulses of 10^{12}–10^{13} protons, separated by at least 2.4 s. Due to this high intensity, the level of radiation background is very high while its decay is exponential ($T_{1/2} \approx$ some ms). In order to be able to detect very short-lived isotopes with low counting rates (for ^{31}Na: $T_{1/2} = 15$ ms and about 3 counts/pulse), the mass selected ions had to be conducted to a detection area which was separated from the target area by a thick shielding (Fig. 6) giving an attenuation of 10^5–10^6 for the background. Furthermore, it was located in a cadmium shielded cage, the purpose of which was to absorb thermalized neutrons, so that the exponential decay was cut off.

E. Total efficiency of the system

From the total thickness of uranium in the target (≈3.4 g/cm^2), the number of protons per pulse and the known cross sections (14 mb for ^{25}Na), the number of produced atoms can be calculated. For ^{25}Na one finds about 10^9 atoms per pulse while the observed number of ions is 10^4. This corresponds to an overall efficiency of 10^{-5}, which is consistent with the value that one obtains using the different reducing factors discussed above and assuming that about 50% of the atoms are extracted from the graphite.

For the sodium isotopes with $A \geq 28$, which have half lives shorter than 60 ms, one has to take into account the delay time between the production of the nucleus and its detection. This delay is due to the diffusion time of the atoms from the graphite and to the ionization time in the mass spectrometer source. A typical time interval for collecting 50% of the ions is 200 ms. The loss due to this delay is about a factor of 7 for a half life of 20 ms (^{31}Na).

IV. EXPERIMENTAL PROCEDURE

Since the optical resonances appear as peaks on a fluctuating base signal, it seemed to be necessary to have a normalization procedure for the beam intensity. Two different normalization procedures have been performed: one with the proton beam intensity and another one with a sodium isotope of the atomic beam. Both normalizations were, however, only 10–20% reliable. The normalization on the proton beam, by measuring the beam intensity using an electrostatic pick up, is subject to error since the production of sodium isotopes depends also upon the focusing of the proton beam on the target oven. The normalization between two sodium isotopes during the same measuring sequence allowed a comparison of the counting rate of a short-lived isotope at the beginning of the diffusion curve with the counting rate of a longer-lived isotope (^{25,26}Na) at the end of its diffusion curve (Fig. 7). But the value of this normalization procedure is limited to about 10% accuracy since for the longer-lived isotopes, counts due to atoms produced during preceding proton pulses were also taken into account.

In practice, the measuring sequence was started by a synchronization pulse from the P.S. preceding the proton pulse by 20 ms. Two ms after the proton pulse, when the background of fast particles had disappeared, ions of the mass A were recorded during a period of 20–300 ms depending on the half life of the isotope. Then, the voltage of the mass spectrometer and the ion beam transport line were set for the longer-lived isotope A' and a measuring period of 1–2 s was started. The corresponding counting rates were stored in buffer counters together with the digitalized fluorescence signal of the ^{23}Na reference beam, the signal of the proton beam intensity from the electrostatic pick up, and the scanning signal of the laser frequency. By a preset counter 1 to 100 cycles could be summed up in the buffer counters for a fixed frequency of the laser. In order to select the best timing for an optimum signal to noise ratio for the A signal, three channels with different counting times were used. The data of the buffer counters were transferred into memories, then read by a PDP 15 computer for analysis of the data and writing on magnetic tapes. Every spectrum started with the recording of at least two resonances of ^{23}Na from the reference atomic beam. Then the laser frequency was changed to allow the recording of the resonances of the sodium isotopes A and A' with an appropriate number of counting cycles per laser step.

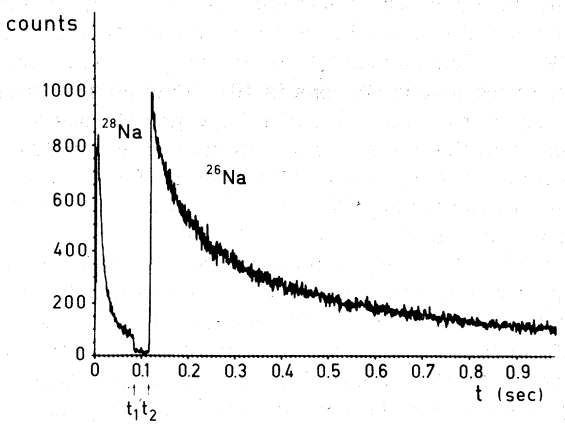

FIG. 7. Diffusion curves for 30 ms ^{28}Na and 1s ^{26}Na. At instant t_1 the mass spectrometer and the ion transport line were changed from mass 28 to mass 26. At instant t_2 counting of mass 26 was started.

V. RESULTS AND DISCUSSION

A. Spins

The spins determined by magnetic resonance for $^{26\text{-}30}$Na are given in Table I. Because of lack of time, the spin for ^{31}Na has not been measured by the magnetic resonance method. The spin assignment for ^{31}Na is based on the value of the hyperfine structure and the isotope shift which indicate that $I=\frac{3}{2}$ is the most probable value. For prolate deformations the eleventh proton should occupy the $\Omega=\frac{3}{2}[211]$ Nilsson model orbit[14] leading to the ground state spin $I=\Omega=\frac{3}{2}$ for the odd isotopes. In the spherical limit the unpaired proton occupies the $d_{5/2}$ shell model orbit and the ground state spin should be $I=\frac{5}{2}$. From this we conclude that spin $\frac{5}{2}$ is a strong indication of an almost spherical nucleus (^{25,27}Na) and that spin $\frac{3}{2}$ indicates prolate deformation (^{21,23,29,31}Na). Assuming for the neutrons the normal filling order of the Nilsson model orbits for prolate deformations (see Fig. 8) the spins of the even isotopes can be explained, except for ^{30}Na. If we take only s-d orbits into account, spin 2 for ^{30}Na can be explained assuming a filled $\frac{3}{2}$ [202] orbit and the unpaired neutron being in the $\frac{1}{2}$ [200] orbit.

B. Magnetic moments

From the observed signals—typical examples are shown in Fig. 9—we first determined the center of gravity of each hyperfine component of the line using a computer program written for the PDP 15. The hyperfine splitting constants A for both the ground state and the excited state derived from this evaluation are given in Table I and are compared to other results when available.

The magnetic moments of $^{26\text{-}31}$Na were calculated from the A factor of the $^2S_{1/2}$ ground state neglecting hyperfine anomaly effects

TABLE I. Spins, hyperfine structure, magnetic moments, and isotope shifts of $^{21-31}$Na. The quoted errors for results of the present work are one standard deviation.

^{x}Na	$T_{1/2}$ [a]	I	$A(^2S_{1/2})$ (MHz)	μ_I (μ_N) corrected	$A(^2P_{1/2})$ (MHz)	$IS^{23,x}$ (MHz)
^{21}Na	22.5 s	$\frac{3}{2}$[b]	953.7(2.0)		102.6(1.8)	−1596.7(2.3)
			953.233(11)[c]	2.38612(10)[c]		
^{22}Na	2.60 y	3[b]	349.3(1.0)		37.5(1.0)	−756.9(1.9)
			348.75(1)[d]	1.746(3)[d]	37.0(1)[e]	−758.5(7)[e]
^{23}Na	stable	$\frac{3}{2}$[b]	885.8130644(5)[f]	2.2175203(22)[f]	94.25(15)[e]	
^{24}Na	15.02 h	4[b]	253.2(2.7)		28.2(2.7)	706.4(6.2)
			253.185018(23)[g]	1.6902(5)[g]		
^{25}Na	60.0 s	$\frac{5}{2}$[b]	882.7(9)		94.5(5)	1347.2(1.3)
			882.8(1.0)[h]	3.683(4)[h]		
^{26}Na	1.07 s	3	569.4(3)	2.851(2)	61.0(3)	1397.5(9)
^{27}Na	290 ms	$\frac{5}{2}$	933.6(1.1)	3.895(5)	100.2(1.1)	2481.3(2.0)
^{28}Na	30.5 ms	1	1453.4(2.9)	2.426(3)	156.0(2.7)	2985.8(2.7)
^{29}Na	43 ms	$\frac{3}{2}$	978.3(3.0)	2.449(8)	104.4(3.0)	3446.2(3.8)
^{30}Na	53 ms	2	624.0(3.0)	2.083(10)	66.2(2.8)	3883.5(6.0)
^{31}Na	17 ms	$\frac{3}{2}$	912(15)	2.283(38)		2486(16)

[a] F. W. Walker, G. J. Kirouac, and F. M. Rourke, Chart of the Nuclides, 12th edition, revised to April 77, distributed by Educational Relations, General Electric Company, Schenectady, N. Y. 12345.

[b] V. S. Shirley and C. M. Lederer, in *Hyperfine Interactions Studied in Nuclear Reactions and Decay* edited by E. Karlsson and R. Wäppling (Almquist and Wiksell, Stockholm, 1975).

[c] O. Ames, E. A. Phillips, and S. S. Glickstein, Phys. Rev. 137, B1157 (1965).

[d] L. Davis Jr., D. E. Nagle, and J. R. Zacharias, Phys. Rev. 76, 1068 (1949).

[e] K. Pescht, H. Gerhard, and E. Matthias, Z. Phys. A281, 199 (1977).

[f] A. Beckmann, K. D. Böklen, and D. Elke, Z. Phys. 270, 173 (1974).

[g] Y. W. Chan, V. W. Cohen, and M. Lipsicas, Phys. Rev. 150, 933 (1966); V. W. Cohen, Bull. Am. Phys. Soc. 18, 727 (1973).

[h] M. Deimling, R. Neugart, and H. Schweikert, Z. Phys. A273, 15 (1975).

$$\mu = \mu_{23}\frac{I}{I_{23}}\frac{A}{A_{23}} \ .$$

The values used for the A factor and the magnetic moment of the reference isotope ^{23}Na are also quoted in Table I. As pointed out above, no theoretical values for the magnetic moments have been reported up to now. Therefore we attempted an interpretation of the magnetic moments in the framework of the Nilsson model[14] using for odd isotopes

$$\mu_I = \frac{I}{I+1}\left[\frac{1}{2}(g_s - g_l) \times \sum_1 (\alpha_{1\,\Omega-1/2}{}^2 - \alpha_{1\,\Omega+1/2}{}^2) + g_l I + g_R\right]$$

and for even isotopes

$$\mu_I = \frac{I}{I+1}\left\{\left[\Omega_p + \frac{1}{2}(g_s^p - g_l^p)\sum_1 (\alpha_{1\,\Omega-1/2}{}^2 - \alpha_{1\,\Omega+1/2}{}^2)^p\right] \pm \left[\frac{1}{2}g_s^n \sum_1 (\alpha_{1\,\Omega-1/2}{}^2 - \alpha_{1\,\Omega+1/2}{}^2)^n\right] + g_R\right\},$$

where the sign of the second term is the same as the sign of Ω_n appearing in the coupling rule $I = \Omega_p \pm \Omega_n$. In the calculation we used $g_s^p = 5.59$, $g_l^p = 1$, $g_s^n = -3.83$, and $g_R = Z/A$. The coefficients $\alpha_{1\,\Omega\pm1/2}$ were taken from Ref. 14. The results are plotted in Fig. 8. Except for ^{25,26,27}Na the magnetic moments are consistent with a positive deformation. For the proton state $\frac{5}{2}$[202] (^{25}Na and ^{27}Na) the calculated moment is deformation independent. But in the case of ^{26}Na the moment indicates an almost spherical shape. It should, however, be noted that the magnetic moments are very sensitive to admixtures of other states to the ground state wave function, therefore the values of the corresponding deformation parameter η, indicated in Fig. 8, have only a limited significance.

C. Isotope shifts

Using the already determined hyperfine structure constants and the nuclear spins the determination of the center of gravity of the D_1 line is straightforward. The results with respect to ^{23}Na are given in the last column of Table I. The consis-

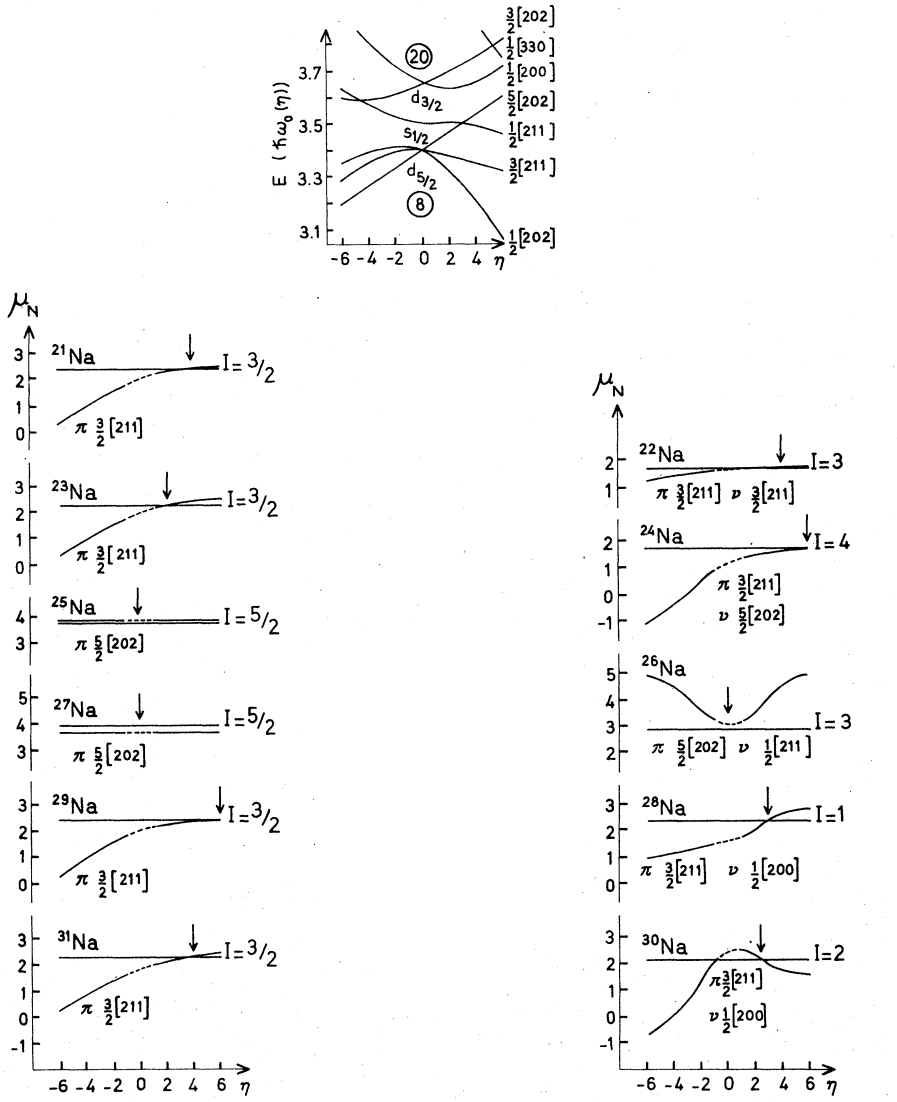

FIG; 8. Nilsson diagram for odd particle levels (Ref. 14), and nuclear magnetic moments of $^{21-31}$Na as functions of the deformation parameter η. The experimental magnetic moments are plotted as straight lines parallel to the η axis, while the Nilsson graph is dashed near the region of zero deformation.

tency between the values of the isotope shift obtained from each of the four hyperfine components of the line was taken into account in the error evaluation. As seen on Table I, the resulting accuracy stands generally between 1 and 3 MHz, which may be considered as characteristic of the experimental set up. In some cases (^{24,30,31}Na) this accuracy was not obtained, owing to occasional difficulties. Because of its 15 h half life, ^{24}Na produces a rather high background when implanted in the first dynode of the electron multiplier, keeping from making further measurements on rarer isotopes. Thus only one measurement was performed on it, and further measurements were planned for the end of the run. But unfortunately this experiment could not be done. In the cases of ^{30,31}Na, the obtained accuracy is not so much due to the low counting rates (10 and 3 counts/pulse, respectively) related to the low production cross sections than to an accidental contamination by hydrocarbons. This means that a new set of measurements could improve the results for these three isotopes very much.

The measured isotope shift is the sum of two effects: the mass shift and the volume shift. The former is divided into a normal mass shift that can be calculated exactly, and a specific mass shift that cannot be calculated with reasonable precision. But both have the same dependence on the nuclear masses

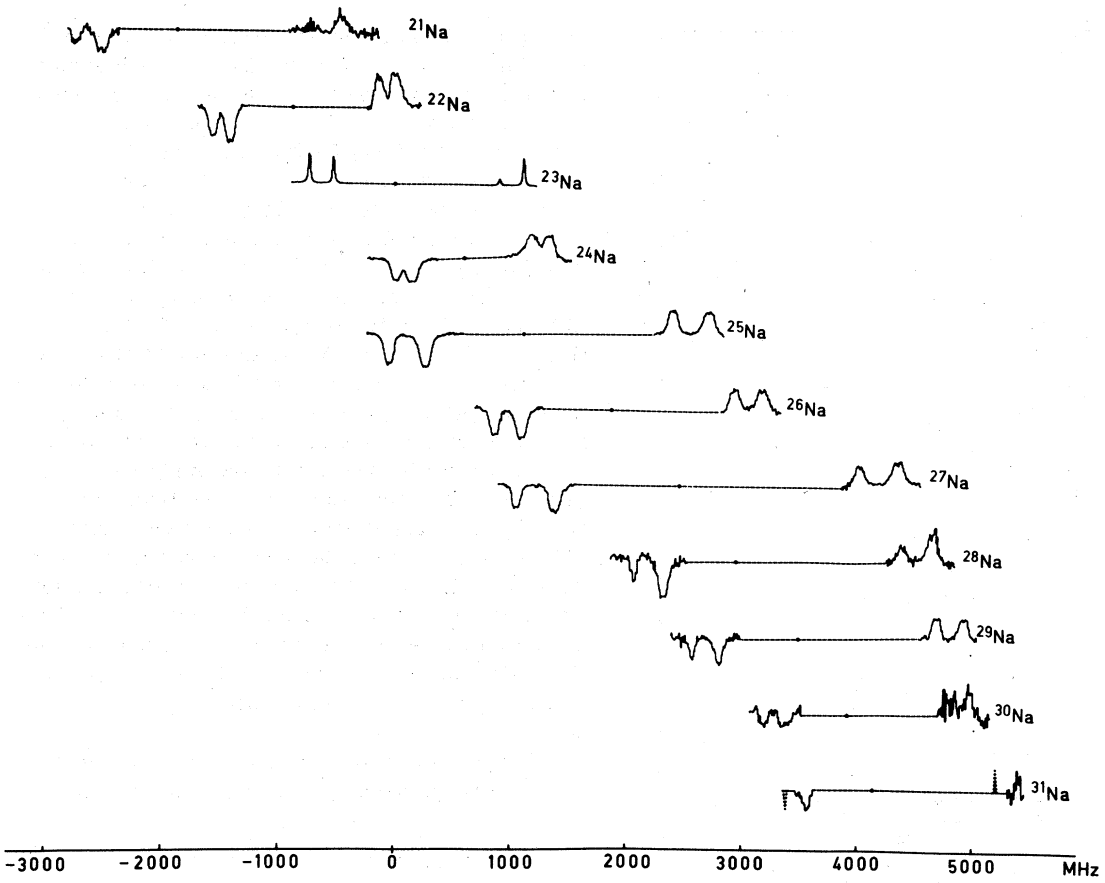

FIG. 9. Hyperfine structure and isotope shifts of $^{21-31}$Na.

$$\delta\nu_{\text{mass}}^{AA'} = K\frac{M_{A'} - M_A}{M_{A'}M_A} \ ,$$

where M_A and $M_{A'}$ are the nuclear masses in atomic mass units and K is the unknown mass shift constant. The volume effect or change in the mean square radius of the nuclear charge distribution has no such mass dependence. For the D_1 line this effect is essentially sensitive for the s electron and may be written

$$\delta\nu_{\text{vol}}^{AA'} \simeq F\delta\langle r^2\rangle^{AA'} \ ,$$

where $\delta\langle r^2\rangle^{AA'}$ is the change in the charge radius and

$$F = (\Pi a_0^3\beta\,|\Psi_s(0)|^2/Z)f(Z) = Ef(Z) \ .$$

$f(Z)$ which takes into account the relativistic corrections to E as well as the finite nuclear charge distribution can be calculated using a formula derived by Babushkin.[15] $|\Psi_s(0)|^2$ is the charge density of the s electron at the nucleus, and a_0 is the Bohr radius. β is a screening factor due to the change in the wave functions of inner closed shell electrons by the valence electron as it changes from $s_{1/2}$ to $p_{1/2}$. β has been determined by Bauche using the Hartree-Fock technique[16]: $\beta = 1.1 \pm 0.1$.

For the light elements the volume shift is not only very small compared to the mass shift but in many cases also negligibly small compared to the experimental errors. Up to now calcium has been the lightest element in which a volume effect has unambiguously been observed.[17-19] Therefore, in the first step of the analysis we only looked for evidence of volume effect contributions to the observed isotope shifts. For this purpose the quantity $\delta\nu_{\text{obs}}^{23,A}M_{23}M_A/(M_A - M_{23})$ has been plotted versus the mass number A (Fig. 10). If the observed isotope shifts were due to a pure mass effect the plotted quantity should be a constant. Therefore we conclude from Fig. 10 that there are volume shift contributions to the isotope shifts well outside the experimental error limits.

The volume shift can also be divided into two parts: the normal volume effect and a deformation effect. For a given change in neutron number the change in nuclear charge radius due to the normal volume effect should be almost constant along the

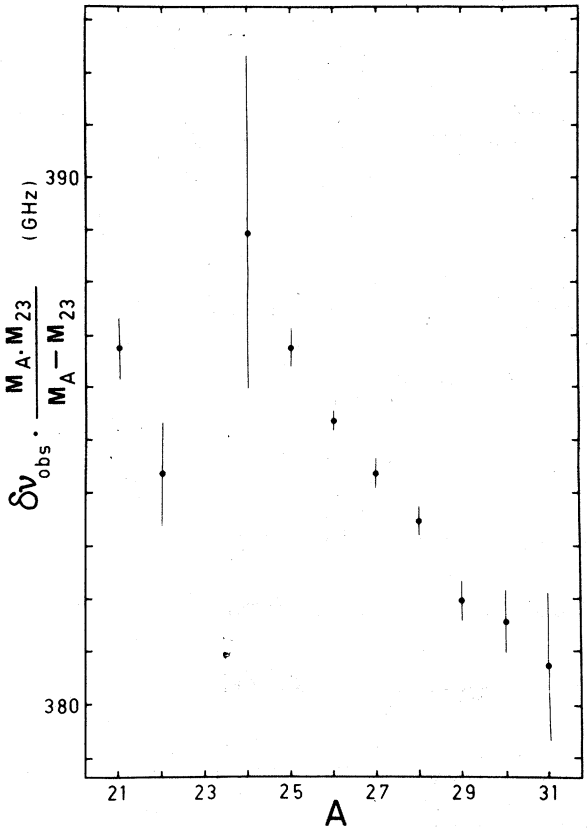

FIG. 10. Evidence of volume effect contributions to the isotope shift of sodium isotopes.

sequence of isotopes of one element, while the deformation effect is proportional to the nuclear deformation and therefore not regular. From Hartree-Fock calculations[2] as well as from the spin $\frac{5}{2}$ of ^{25}Na and ^{27}Na and from the magnetic moment of ^{26}Na, we tentatively make the assumption that for ^{26,27}Na the volume shift with respect to ^{25}Na can be described by the normal volume effect

$$\delta\nu_{vol}^{AA'} = F \times \zeta \times \delta\langle r^2\rangle_{std}^{AA'},$$

where

$$\delta\langle r^2\rangle_{std}^{AA'} = \tfrac{2}{5} r_0^2 \delta A / \overline{A}^{1/3}$$

and

$$\delta A = A' - A, \overline{A} = (A + A')/2.$$

$\delta\langle r^2\rangle_{std}$ is the change of nuclear charge radii for uniformly charged sphere of standard radius $R = r_0 A^{1/3}$ ($r_0 = 1.2$ fm). $\zeta \leq 1$ is the so-called isotope shift "discrepancy" describing the fact that the radius of the nuclear charge distribution of a spherical nucleus increases less rapidly than $A^{1/3}$ when neutrons are added. This can be understood in terms of the dependence of the proton potential on the neutron excess.[20] Since for the present case ζ is unknown, we performed the following calculations for $\zeta = 1$ and for $\zeta = 0.5$ which should be the upper and lower limit as it has been found for elements with $Z \geq 19$.[21,22] $\zeta \approx 0.5$ is also consistent with Hartree-Fock calculations.[2]

From the hyperfine structure of the ground state of ^{23}Na we find $|\psi_s(0)|^2 = 0.75 a_0^{-3}$ and $E = 0.326$; $f(Z) = -199$ MHz/fm^2 is calculated from an expression given by Babushkin,[15] and as the final result for the volume shift constant we obtain $F = -47$ MHz/fm^2. From the isotope shifts of $^{25\text{-}27}$Na we then find the mass shift constant $K = 388$ GHz for $\zeta = 1$ and $K = 385$ GHz for $\zeta = 0.5$, and using the mass factors $(M_{A'} - M_A)/M_{A'} \cdot M_A$, the volume shift for the other isotopes was evaluated. The results are shown in Fig. 11. Both curves show the same general trend: deviations from the lines $\delta\langle r^2\rangle_{std}$ and $\frac{1}{2}\delta\langle r^2\rangle_{std}$ respectively, for the light isotopes $^{21\text{-}24}$Na as well as for the heavy isotopes starting with ^{28}Na. It should be noted that these deviations would be true for any reasonable value of ζ. They can be interpreted as an effect of nuclear deformation. For the light isotopes such a deformation is already well documented (see, e.g., Refs. 20, 23).

Although this analysis of the isotope shifts is based on rough assumptions it should give the

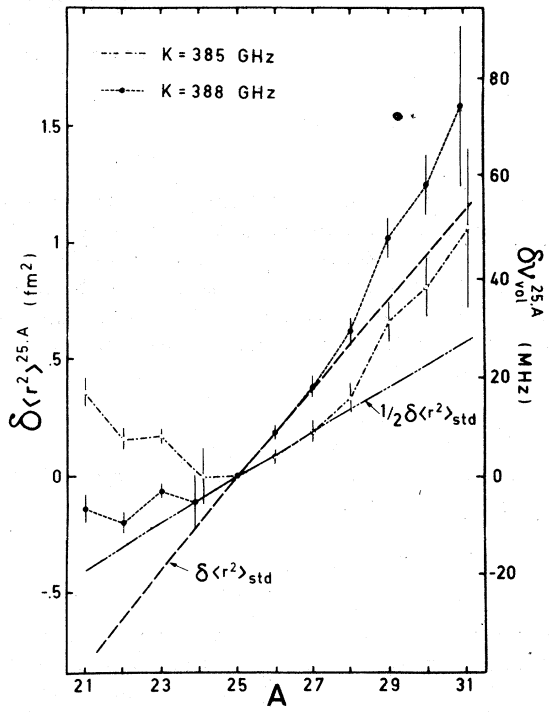

FIG. 11. Differences of mean square nuclear charge radii with respect to ^{25}Na for two values of the mass effect constant K. The error bars are due only to the experimental uncertainties.

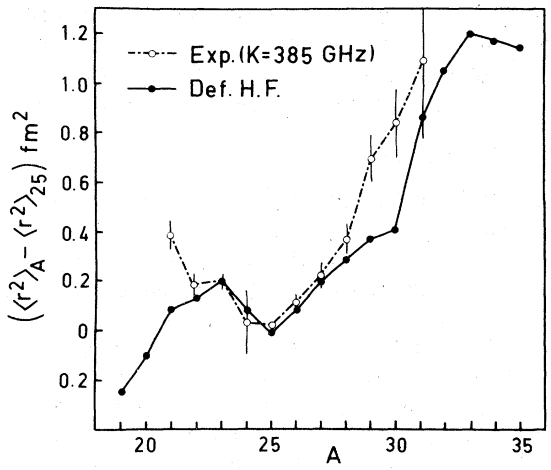

FIG. 12. Comparison of experimental values for the change in the mean square nuclear charge radius (for K = 385 GHz) and of values obtained from deformed Hartree-Fock calculations (from Ref. 2.).

right order of magnitude for the specific mass shift. For the isotope pair 23-25 we obtain from $K = 385$ GHz a total mass effect of 1341 MHz, and after subtracting the normal mass shift which can be calculated exactly (see, e.g., Ref. 18) we find a specific mass shift of about 370 MHz which is large compared to a theoretical value of 60 MHz calculated with the Hartree-Fock technique.[24] The mean square charge radii extracted from the isotope shift data can be compared to values derived from deformed Hartree-Fock calculations.[2] The $\delta\langle r^2\rangle$ values obtained when assuming an isotope shift "discrepancy" $\zeta = 0.5$ are in good agreement with the calculated ones for $^{23\text{-}28}$Na and ^{31}Na. Between ^{28}Na and ^{31}Na the experimental curve increases more monotonically than the theoretical curve which shows a sudden increase at ^{31}Na (see Fig. 12).

VI. CONCLUSION

The present investigation extends the data on spins and magnetic moments to the sodium isotopes $^{26\text{-}31}$Na. The comparison to Nilsson model calculations gives some estimates on nuclear deformation. From the precise determination of the isotope shift of the D_1 line of the isotopes $^{21\text{-}31}$Na, clear evidence of volume shift contributions is obtained. The interpretation in terms of nuclear charge radius changes also gives information on nuclear deformation, although there remains the uncertainty introduced by the specific mass effect. The information on nuclear deformation extracted from the isotope shifts is in agreement with those obtained from spins and magnetic moments. Indeed, the spins and magnetic moments as well as the charge radii indicate prolate deformation for $^{21\text{-}24}$Na, lying in an already well established region of positive deformation, and also for $^{28\text{-}31}$Na, while $^{25\text{-}27}$Na may be considered as having almost spherical nuclei.

To check this analysis of nuclear deformation, further measurements are required. Measurements in the neighboring elements Mg and Ne should exhibit a similar structure of the nuclear radius changes. A determination of the static quadrupole moments of the sodium isotopes by measuring the hyperfine structure of the D_2 line is planned and should give further information on nuclear deformation. An improved accuracy in the ^{30}Na and ^{31}Na isotope shift measurements and an extension to ^{32}Na (for which according to the production cross section only 0.2 counts per proton pulse are expected) should clarify the structure in the changes of charge radii around the neutron number $N = 20$.

ACKNOWLEDGMENTS

It is a pleasure to acknowledge the able assistance of R. Fergeau, M. Jacotin, and J. F. Kepinski in building and setting up the mass spectrometer, and related equipment and shielding, as well as maintaining it during the run. We are indebted to C. Vialle for the excellent contribution in maintaining a stable laser operation. We thank G. Le Scornet for writing the computer programs on PDP 15, B. Rosenbaum for building the data acquisition system, J. Biderman and D. Barbet for making the target and ionizer, and R. Baronnet for building the ^{23}Na reference atomic beam apparatus. We thank A. Ball, J. M. Michaud, J. Zaslavsky, and all the members of the Experimental Facilities Division and of the P.S. staff for maintaining the high intensity proton beam. One of us (S.B.) wishes to acknowledge receipt of a fellowship from the Deutsche Forschungsgemeinschaft.

APPENDIX A: PRINCIPLE OF CALCULATIONS OF THE OPTICAL PUMPING

For the hyperfine component $^2S_{1/2}, F - {}^2P_{1/2}, F'$ of the D_1 line the evolution of the populations of the Zeeman sublevels of the ground state is given by the equations

$$\frac{dp_m}{dt} = -p_m \sum_M (1 - E_{Mm}) \frac{A_{mM}}{T_p} + \sum_M \sum_{m' \neq m} \frac{E_{Mm} A_{m'M}}{T_p} p_{m'},$$

$$\frac{dp_{\bar{m}}}{dt} = \sum_M \sum_m \frac{E_{M\bar{m}} A_{mM}}{T_p} p_m,$$

where the quantum numbers m and M denote the Zeeman sublevels of the hyperfine levels F and F', respectively, and $\bar{m}$ denotes the sublevels of the ground state hyperfine level not involved in

the transition. A_{mM}/T_p is the absorption probability per unit time, where

$$A_{mM} \propto \begin{pmatrix} F & 1 & F' \\ -m & q & M \end{pmatrix}^2 (2F+1)(2F'+1) \begin{Bmatrix} F & 1 & F' \\ J' & I & J \end{Bmatrix}^2 ,$$

with $q = \pm 1$ for σ^- or σ^+ light. The pumping rate $1/T_p$ is proportional to the light power density W.[25] E_{Mm} is the emission probability from the excited sublevel M to the ground state Zeeman sublevel m. We normalize the E_{Mm} as

$$\sum_m E_{Mm} + \sum_{\bar{m}} E_{M\bar{m}} = 1 .$$

APPENDIX B: TRANSMISSION OF THE SIX-POLE MAGNET

In the strong magnetic six-pole field the nuclear spin and the electronic angular momentum are decoupled. The sodium atoms have either $m_J = +\frac{1}{2}$ or $m_J = -\frac{1}{2}$ with the corresponding effective magnetic moment $\mu_{\text{eff}} = \pm\mu_B$. Then it can be shown[26] that in the inhomogeneous six-pole field, in which the atoms are submitted to a radial force, the atoms with $m_J = +\frac{1}{2}$ follow a sinusoidal trajectory and those with $m_J = -\frac{1}{2}$ an hyperbolic one.

The angular frequency of the harmonic oscillation depends on μ_{eff}, on the atomic mass m, and on the characteristics of the magnet used. The transmission of the six-pole magnet is conveniently described by the transmission solid angles Ω^+ and Ω^- for $m_J = \pm\frac{1}{2}$. To calculate these quantities we follow the considerations developed in Ref. 26

$$\Omega^+(\eta) = \Pi[X_0^+(\eta)]/L ,$$

where $X_0^+(\eta)$ is the maximum transverse entrance coordinate insuring that throughout the magnet length the transverse deviation is smaller or equal to the magnet radius gap. $X_0^+(\eta)$ is calculated from the equation of motion. L is the distance from the atomic beam source to the magnet entrance. η is defined as $\eta = \alpha\sqrt{2}/V$, $\alpha = (2kT/m)^{1/2}$. $\Omega^-(\eta)$, for atoms in the state $m_J = -\frac{1}{2}$ is similarly defined. The efficiency of the six-pole magnet as a state selector is defined by a parameter s

$$s = \frac{N^+ - N^-}{N^+ + N^-} ,$$

where

$$N^\pm \propto \int_0^\infty F_{\text{beam}}(\eta)\Omega^\pm(\eta)d\eta .$$

$F_{\text{beam}}(\eta)$ is the beam velocity distribution. N^+ and N^- are the number of transmitted atoms in the state $m_J = +\frac{1}{2}$ and $m_J = -\frac{1}{2}$, respectively, averaged over the velocity distribution of the beam.

---

†Presently at Gesellschaft für Schwerionenforschung—D 6100 Darmstadt 1, Germany
‡On leave from University of Bonn, Bonn, Germany

[1]C. Thibault, R. Klapisch, C. Rigaud, A. M. Poskanzer, R. Prieels, L. Lessard, and W. Reisdorf, Phys. Rev. C 12, 644 (1975).
[2]X. Campi, H. Flocard, A. K. Kerman, and S. Koonin, Nucl. Phys. A151, 193 (1975).
[3]C. Thibault, G. Audi, M. Epherre, G. Huber, R. Klapisch, and F. Touchard (unpublished).
[4]C. Détraz, D. Guillemaud, G. Huber, R. Klapisch, M. Langevin, F. Naulin, C. Thibault, L. C. Carraz, and F. Touchard, Phys. Rev. C (to be published).
[5]B. J. Cole, A. Watt, and R. R. Whitehead, J. Phys. A 7, 1399 (1974).
[6]H. T. Duong and J. L. Vialle, Opt. Commun. 12, 71 (1974).
[7]G. Huber, C. Thibault, R. Klapisch, H. T. Duong, J. L. Vialle, J. Pinard, P. Juncar, and P. Jacquinot, Phys. Rev. Lett. 34, 1209 (1975).
[8]G. Huber, R. Klapisch, C. Thibault, H. T. Duong, P. Juncar, S. Liberman, J. Pinard, J. L. Vialle, and P. Jacquinot, C. R. Acad. Sc. Paris, B282, 119 (1976).
[9]A. M. Poskanzer, G. W. Butler, and E. K. Hyde, Phys. Rev. C 3, 882 (1971).
[10]C. Thibault-Philippe, thesis, Orsay, 1971 (unpublished).
[11]C. Thibault, G. Huber, G. Audi, M. Epherre, D. Guillemaud, R. Klapisch, F. Naulin, and F. Touchard, (unpublished).
[12]P. Juncar and J. Pinard, Opt. Commun. 14, 438 (1975); P. Juncar, thesis, Orsay, 1976 (unpublished).
[13]W. Weiershausen, Ann. Phys. (Leipzig) 15, 252 (1965); in *Advances in Mass Spectrometry*, edited by W. L. Mead, (The Institute of Petroleum, London 1966), Vol. 3, p. 755.
[14]S. G. Nilsson, K. Dan. Vidensk. Selsk. Mat. Fys. Medd. 29, No. 16 (1955).
[15]F. A. Babushkin, Zh. Eksp. Teor. Fiz. 44, 1667 (1963). [Sov. Phys. JETP 17, 1118 (1963)].
[16]J. Bauche, private communication.
[17]R. Neumann, F. Trager, J. Kowalski, and G. zu Putlitz, Z. Phys. A279, 249 (1976).
[18]K. Heilig and A. Steudel, At. Nucl. Data Tables 14, 613 (1974).
[19]J. Bauche and R. J. Champeau, in *Advances in Atomic and Molecular Physics* (Academic Press, New York, 1976), Vol. 12.
[20]A. Bohr and B. R. Mottelson, *Nuclear Structure* (Benjamin, New York, 1969), Vol. 1.
[21]R. L. B. Elton, *Landolt-Börnstein: Nuclear Radii*, edited by H. R. Collard, R. L. B. Elton and R. Hofstadter (Springer, Berlin, 1967), New Series, Group I, Vol. 2.
[22]J. Bonn, G. Huber, H. J. Kluge, and E. W. Otten, Z. Phys. A276, 203 (1976).

[23]J. M. Eisenberg and W. Greiner, *Nuclear Theory* (North-Holland, Amsterdam, 1975), Vol. 1.
[24]J. Bauche, J. Phys. 35, 19 (1974).
[25]C. Cohen-Tannoudji and A. Kastler, in *Progress in Optics*, edited by E. Wolf (North-Holland, Amsterdam, 1966), Vol. V.
[26]V. Hughes, R. L. Long, Jr., M. S. Lubell, M. Posner, and W. Raith, Phys. Rev. A 5, 195 (1972).